

# Techniques for Schumann Resonance Measurements: A Comparison of Four Amplifiers with a Noise Floor Estimate

José A. Gázquez, *Senior Member, IEEE*, Manuel Fernández-Ros, Nuria Novas and Rosa García

**Abstract**— Schumann resonances are very weak natural electromagnetic signals, produced in the Earth-ionosphere cavity are located in the ELF band (7 to 60Hz), and the sensors that measure them produce amplitudes of few microvolts. Strong signals from power lines (50 to 60Hz) occur in the same frequency range. Amplification techniques play a key role in acquiring resonance modes with the best signal-to-noise (S/N) ratio. This paper presents a study of the various structures of amplification systems that optimize the S/N ratio for the signal of interest. The aim of this study is to measure all possible resonance modes with low time acquisition. To this end, we compare four instrumentation amplifiers and design a new indirect method for obtaining the noise floor of the system with sensors manufactured on magnetic cores that are several meters long. We present the measurements of the Schumann resonance achieved using these techniques at the ELF electromagnetic wave observatory at Calar Alto (Spain). The solutions adopted allow to measure seven resonance modes with acquisition times of 30 minutes, where the S/N ratio in the fundamental mode was 39dB.

**Index Terms** –ELF band, instrumentation amplifier, noise, Schumann resonance, measurement, magnetic sensor.

## I. INTRODUCTION

THE electromagnetic waves due to natural phenomena and human activity that reach the earth's surface cover a wide range of frequencies in the spectrum. In the extremely low frequency (ELF) range, the 5 to 100 Hz band is associated with a phenomenon known as the Schumann resonance [1]. This phenomenon occurs in the cavity formed by the Earth's surface and the ionosphere, which acts as a waveguide for ELF signals arising from electrical activity in the atmosphere [2]. Measurement of this phenomenon allows characterization and diagnosis of the terrestrial environment [3] as well as the calibration of global temperature [4]. It can also be considered a tool for preventing earthquake disasters [5] and for measuring lightning activity [6] and the average conductivity of the earth's ionosphere [7]. This natural phenomenon can also be applied to investigate the electromagnetic environment of other planets in the solar system and to provide information on climate and other properties of the lower part of any planet that has an ionosphere [8].

The majority of published papers are related to the study of ELF wave propagation in the Earth-ionosphere cavity,

demonstrating the complexity of the measurement process and amongst other factors, the non-uniformity of the ionosphere, the presence of natural electromagnetic noise [9], the presence of interference in industrial areas, and background noise [10]. Studies tend to present the spectral characteristics of the resonance models and their amplitude [11], making comparisons between observed data and theoretical models of components for the magnetic field associated with the phenomenon [12] as well as variations in the signals, depending on local and universal time [13].

These studies consider only the first three resonance modes, located in the frequency range 7 to 28 Hz [14]. Occasionally, capture extends to the fourth mode [15] although, under extreme conditions of nearby lightning strikes, up to 13 modes have been observed [16].

Very few publications give any indication of the general aspects of the measurement system used, given that they should be comprised of a receiving magnetic loop antenna, low-noise amplifier, low-pass filter, an A/D converter and a datalogger [17]. A recent publication [18] presented descriptively a measuring station of Schumann resonances in Mexico but no details of measurement electronics are given. In no instance do the authors consider problems such as those arising from the electrical characteristics of the sensor, its adaptation to the amplification system, the structure and analysis of the amplification system, or the low-level signal obtained. In addition, they do not provide data regarding the noise where the signal is embedded, the signal-to-noise (S/N) ratio of the measured signal or the method for obtaining it. Moreover, several hours or days are usually needed to provide relevant data from the ELF signals [11] without regard to the benefits to be achieved by reducing the averaging time because long records of resonances can vary over the acquisition time, leading to an incorrect assessment of the results. The need to reduce the noise in spectral estimation techniques is a topic of current interest [19]. A solution would be to reduce the amplifier noise to a possible minimum. Some authors propose methods of reducing noise through an amplifier by using a field effect transistor (FET) preamplifier [20][21]. Other recent studies are focused on noise reduction in amplifiers coupled by capacitor [22]. But an evaluation of the signal-to-noise ratio is indispensable for obtaining quantitative rather than qualitative assessments of ELF signals. Optimization of the amplification system will enable an improvement of the signal-to-noise ratio and a reduction in the capture time needed for their analysis in the frequency domain.

To study the ELF electromagnetic waves, the University of

Copyright statement: © 2015. Parra, J. A. G., Ros, M. F., Castellano, N. N., & Salvador, R. M. G. (2015). Techniques for Schumann resonance measurements: a comparison of four amplifiers with a noise floor estimate. IEEE Transactions on Instrumentation and Measurement, 64(10), 2759–2768. doi: 10.1109/TIM.2015.2420376. Personal use of this material is permitted. Permission from IEEE must be obtained for all other uses, in any current or future media, including reprinting/republishing this material for advertising or promotional purposes, creating new collective works, for resale or redistribution to servers or lists, or reuse of any copyrighted component of this work in other works.

Almeria designed the first observatory of ELF waves in Spain at Calar Alto (Almeria province) and began operation in 2011. The observatory consists of two magnetic antennas, oriented north-south (NS) and east-west (EW). Each antenna consists of two symmetrical windings, providing balanced differential signals to minimize common mode effects [23].

The off-line study undertaken at the Universidad de Almeria estimated the spectral density based on fast Fourier transform (FFT) algorithms using averaged periodograms [24].

A complex study for measuring the Schumann resonances is required to correctly quantify the measurements and optimize the time averaging. By developing these systems, the efficiency of capture of the signals coming from the Schumann resonance will be improved, thereby facilitating their subsequent study and analysis.

The present study has the following objectives:

1. Design an optimal amplification system for measuring ELF signals and, in particular, the Schumann resonances. This system must meet certain specifications, such as low noise, minimal intermodulation, filtering of power line signals, and it must use techniques that improve the overall dynamic range of the system.
2. Perform a comparison from a noise perspective using four instrumentation amplifiers supplied by three leading manufacturers.
3. Design a new method for obtaining the noise floor of the system, which allows an assessment of the signal-to-noise ratio of the signals obtained and sensors manufactured on magnetic cores that are several meters long.

## II. ELF SENSORS AND INTRINSIC NOISE

The structure of the measurement system needs to consider the characteristics of the sensors that comprise it because these elements act as the source of the signal for the system. Because of the frequency range to be measured, the sensors usually used are coils with a magnetic core and a large number of windings with high internal impedance that is dependent on the operating frequency. Fig. 1 shows the classic model of a sensor coil and its series equivalent circuit.

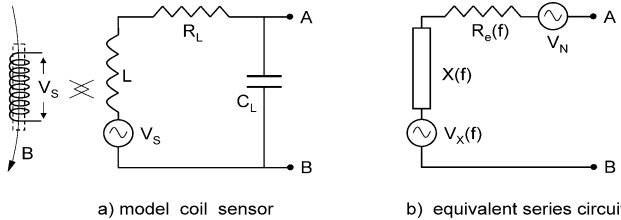


Fig. 1. Model of a sensor coil.

As it crosses a solenoid  $L$ , the magnetic field  $B$  induces an electrical voltage  $V_s$  in accordance with Faraday's law (1), where  $A$  is the surface area of the solenoid and  $n$  is the number of windings.

$$V_s(t) = A \cdot n \cdot \frac{dB}{dt} \quad (1)$$

In the case of sinusoidal signals:  $B(t) = \bar{B} \cdot \sin(\omega t)$ , the induced voltage is expressed by (2).

$$\bar{V}_s(\omega) = A \cdot n \cdot \omega \cdot \bar{B} \quad (2)$$

Because of the dependence of the induced signal on factor  $\omega \cdot \bar{B}$ , a cored coil with a large number of turns in the ELF range cannot be modeled; thus no formal relationship can be obtained between the voltage induced by the magnetic field,  $V_s$  (from Fig. 1a) and the voltage of the generator  $V_x(f)$  of the series equivalent circuit of the sensor (Fig. 1b). To establish this relationship, we have to study the response of a "source-sensor-amplifier" system, as described in section III. The correct characterization of the sensor in terms of adaptation and noise requires the experimental measurement of the impedance versus frequency  $Z(f)$  to determine the adaptation characteristics and the spectral density of the noise. The noise can be modeled in the series equivalent circuit using a generator  $V_N(f_i)$ , which is a function of the real part of the impedance  $Re[Z(f)]$  and the frequency (3).

$$V_N(f_i) = \sqrt{4KT \operatorname{Re}[Z(f_i)]} \quad (3)$$

$K$ : Boltzmann constant;  $T$ : temperature in Kelvin degrees.

Trials were established using three balanced sensors and a high-permeability core. Table I shows the most important characteristics:  $\Phi$  is the diameter of the thread,  $n$  is the number of windings,  $l_{core}$  is the length of the core,  $R_L$  is the resistance of the sensor in DC and  $L$  is the inductance at 5 Hz, considering a single section of the balanced coil.

TABLE I  
SENSOR CHARACTERISTIC

Sensor	$\Phi$ (mm)	$n$	$l_{core}$ (m)	$R_L$ (K $\Omega$ )	$L$ (H)
Sensor 1	0.5	29225+29225	2	1.35	479
Sensor 2	0.5	29225+29225	2	1.35	943
Sensor 3	0.15	150000+150000	2	34	11632

The difference between sensors 1 and 2 is their self-resonance: in sensor 1, self-resonance is far away from the 0 to 100 Hz range, and this enables measurements of up to 1 KHz. Moreover, sensor 2 is resonant at 7.5 Hz and is only suitable for high resolution measurements of the first Schumann resonance mode. Sensor 3 was designed so that it has a bandwidth of 0 to 100 Hz.

### A. Characterization of the Sensor

Characterization of the ELF sensors was performed using a vector network analyzer (VNA), model E5061B (Agilent). The most direct method for measuring an impedance  $Z$  using a VNA is by measuring the  $S_{11}$  port, which provides a direct ratio with  $Z$ . Using this method, the higher the impedance, the larger the error because  $Z$  is measured in relation to the characteristic impedance  $Z_0$ . For values of impedance of hundreds of K $\Omega$ , the error invalidates the measurement. Another method consists of using the impedance  $Z$  as a quadrupole between the two ports of the VNA and measuring the transmission parameter  $S_{21}$  [25]. This parameter is given in equation (4) from which the impedance  $Z$  is obtained by means of expression (5).

$$S_{21} = \frac{2Z_0}{Z + 2Z_0} \quad (4)$$

$$Z = 2Z_0 \left( \frac{1}{S_{21}} - 1 \right) \quad (5)$$

This method was used for values of  $Z$  greater than  $5 \text{ M}\Omega$ . It has very little error in the low-frequency range and is considered adequate for characterizing sensors that have a large number of fine windings, such as sensor 3.

The real part of the sensors impedance depends on the frequency. Fig. 2 compares the impedance module of each sensor ( $Z$ ) and the real part of this impedance ( $Re(Z)$ ). One can see that in sensor 3, there is close coincidence between  $Z$  and  $Re(Z)$ ; likewise, in sensor 2 even though here, the coincidence is not as close. In contrast, the divergence in sensor 1 spans an order of magnitude.

Based on the experimental impedance curves of the sensor, we can represent  $V_N(f_i)$  and calculate the total noise that it introduces into the measurement frequency range.

Fig. 3 compares the spectral density of thermal noise from the sensors connected to an amplifier with an input impedance of  $5 \text{ M}\Omega$ . We can see that in sensor 3 (with its large number of turns of fine wire) there is greater thermal noise than in the other sensors, which have a shorter length of thicker copper wire.

The total noise  $V_{NT}$  is calculated numerically for a particular temperature, given that the vectors for the real part of the impedance  $Re[Z(f)]$  increase as the frequency increases (6):

$$V_{NT} = \sum_{f=f_1}^{f_2} \sqrt{4KT Re[Z(f)] \cdot \Delta f} \quad (6)$$

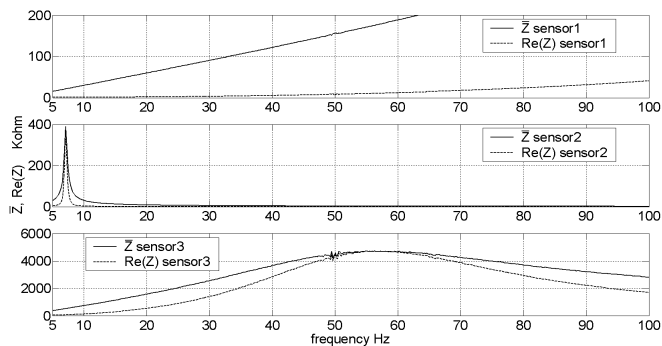


Fig. 2. Comparison of sensors in terms of the  $Z$  module and its real part  $Re(Z)$ .

where  $f_1$  and  $f_2$  are the lower and upper frequencies of the range in which the total noise of the sensor is determined and  $\Delta f$  is the frequency increment of vector  $Re[Z(f)]$ . Knowing the total noise of the sensor, we can determine the equivalent noise resistance  $R_{Neq}$  (7). This parameter is useful for comparing the noise of the sensor with the noise of the amplifier within the frequency range being studied,  $B = f_2 - f_1$ :

$$R_{Neq} = \frac{V_{NT}^2}{4KTB} \quad (7)$$

where  $K$  represents the Boltzmann constant and  $T$  is the temperature.

The total noise obtained at  $300^\circ \text{ K}$  in sensor 1 was  $0.20 \mu\text{V}$ . In sensor 2, it was  $0.11 \mu\text{V}$  and in sensor 3, it was  $2.5 \mu\text{V}$ . The noise in sensor 3 is an order of magnitude higher than the others, even though this factor does not determine the efficiency of the measurements because the sensor may deliver a greater signal level than the others. To determine the quality of the

measurements, it is necessary to compare the signal measured against the total noise of the system.

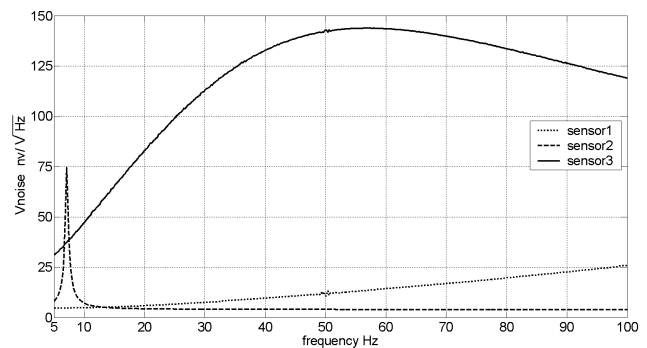


Fig. 3. Spectral density of noise for sensors connected at  $5 \text{ M}\Omega$ .

### III. AMPLIFICATION SYSTEM

The amplification system is heavily dependent on the input impedance, sensitivity and noise because of the characteristics of the sensor, which will determine its structure and gain.

#### A. Impedance Matching of the Sensor-Amplifier

With respect to the adaptation of the sensor-amplifier, it is very important to study the impedance of the sensors as a function of frequency. The loading effect on the sensor-amplifier and the noise generated in the system are conditioned by the dependence of the real part of the sensor's impedance on frequency. Therefore, the value of the direct current resistance of the sensor is not a valid value. (see Fig. 2).

On the basis of the impedance data from the sensors studied, the need for a first amplifier stage with high input impedance and low noise is confirmed, and an instrumentation amplifier is the most suitable for this stage.

According to the data in Fig. 2, the dominant part of the impedance is the real part, and it is not appropriate to establish a passive network that fits the imaginary part because the detriment in the nonlinear response does not compensate for the improvement in insertion.

To determine the insertion losses for each case, we need to numerically solve for the attenuation value as a function of the frequency. Fig. 4 shows the insertion losses of the three sensors with respect to frequency, connected to an amplifier with a  $5 \text{ M}\Omega$  input resistance. This value might be considered high, but note that the standard oscilloscopes have an input resistance of  $1 \text{ M}\Omega$ , and  $10 \text{ M}\Omega$  with a  $\times 10$  attenuator probe.

Sensor 3 exhibits the greatest insertion losses and is greater than  $5 \text{ dB}$  at certain frequencies, while sensors 1 and 2 do not show any appreciable losses. In view of the above results, it is clearly important that the input impedance of the first amplifier stage has a value high enough to avoid the loss of a large proportion of the energy delivered by the sensor when connecting to the amplifier.

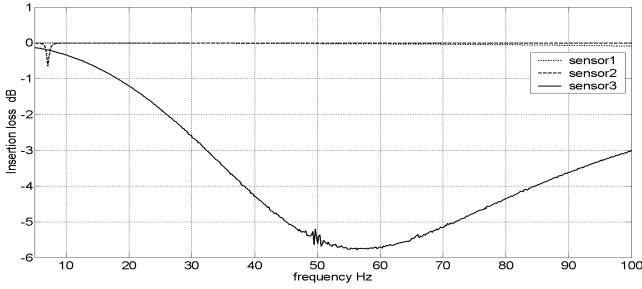


Fig. 4. Insertion losses of the sensors with  $Z=5\text{ M}\Omega$ .

### B. Sensor-Amplifier Transmission Line

The connection of the sensor to the amplification system will always be in differential mode. Non-differential connections imply a significant degradation of the signal due to the capture of common mode signals because the cable acts as an electrical antenna. For the differential connections, the unbalanced configuration (Fig. 5a) has the drawback of the sensor-amplifier connection cable capturing unwanted signals, thus constraining its length. This problem is typical for cases of stage adaptation for audio [26], whereas selecting balanced configurations (Fig. 5b) allows a cable length of 10 m without attracting unwanted signals. In field trials, we discovered the benefit of using a balanced configuration, which allowed a cable length of 10 m without increasing the level of interference from the main supply. The sensor was grounded using a copper peg because without this, we captured signals generated by instruments used during the set up of the installation, such as portable oscilloscopes. The electrical effect of the cable can be modeled by only considering the value of the distributed capacitor  $C_C$  presented by a cable, in parallel with the sensor output with a value proportional to the length of the cable in which case, the use of cables with low distributed capacitance ( $<100\text{ pF/m}$ ) is advisable. The distributed effects in transmission lines in the ELF band are negligible for lengths of a few tens of meters. Fig. 5 shows different connection configurations.

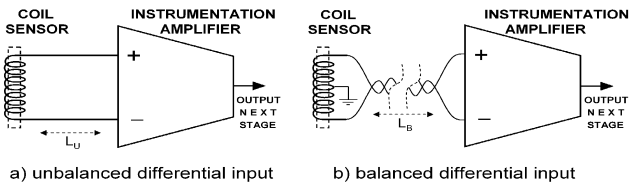


Fig. 5. Connection between the sensor and first-stage amplifier.

### C. Amplification Stage

The most suitable structure for the first-stage amplification, with a specification for a high-input impedance ( $Z > 1\text{ M}\Omega$ ) and high gain ( $G > 60\text{ dB}$ ) corresponds to an instrumentation amplifier.

The tests undertaken lead us to believe that the system will require a gain of between 60 dB and 110 dB. The first stage can provide a gain of up to 60 dB without instability problems. To achieve the remaining gain, a second amplification/conditioning stage is required and does not demand a high-quality instrumentation amplifier so that two

low-noise, high precision operational amplifiers are sufficient. Fig. 6 shows the overall structure of the system.

The measurement system includes an optional notch filter implemented using an active cell in double T [27] to attenuate the signal from the main supply (Fig. 6). The filter is inserted between the two amplification stages to prevent the degradation of the overall noise figure, even though this filter is optional. This type of filter is useful when taking measurements close to power lines or when the high intensity of signals from the power lines, captured by the sensor, saturate the dynamic range to produce minimal gain because it has a negative effect on the linearity of the data and poses problems around the suppressed frequency.

During the development of this system, four instrumentation amplifiers were tested. The models tested were AD524 [28], INA110 [29], INA126 [30] and LT1167 [31]. These models are, currently, the most relevant devices of different brands, and they range from very low-cost amplifiers (INA126) to the most expensive amplifiers, including top of the range (AD524). Amplifiers AD524 and INA110 feature an integrated resistance setting that can access preset gains without the need for external components. Fig. 7 is a scheme of the internal make-up of amplifier AD524. In addition, the noise sources of these resistances can be included; these sources are among the features provided by the manufacturers. The LT1167 and INA126 models are instrumentation amplifiers that require additional external resistances to fix their gain. The internal configurations of amplifiers INA110, INA126 and LT1167 are traditional with three operational amplifiers (OA), while amplifier AD524 is configured with five OAs, which means it has a broader bandwidth (Fig. 7).

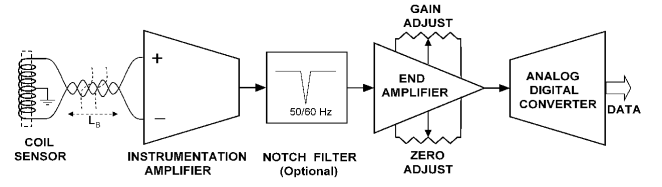


Fig. 6. Structure of the measurement system.

For amplifiers AD524 and INA110, the maximum gain possible was selected for their internal resistances, 60 dB and 54 dB, respectively. For amplifier LT1167, a gain of 60 dB was selected and for amplifier INA126, a gain of 54 dB was selected. We limited the gain of these amplifiers to 60 dB because of the instability problems encountered during the tests. The high gain used for each of the devices together with the high impedance of the sensors led to the use of input resistances of  $5\text{ M}\Omega$  for all of the amplifiers, and the AD524 amplifier was the one with the greatest tendency for instability as the resistance seen by the inputs increased.

The selection of these high gain values causes the band of the amplifier to be limited, but it is not possible to use capacitors because of the lack of access to the internal resistances in models AD524 and INA110. One solution to resolve the band limitation is to introduce an inductor in series with  $R_I$  (Fig. 7). According to (8), a pole is introduced at  $S = S_I$ . In the circuit,  $L$  has a value of 60 mH, which situates the pole at approximately 100 Hz. The inductor is made of a material called T38 around a

ring core, which means it has a small size, few windings and an insignificant internal resistance in comparison to  $R_I$ . In addition, the ring core minimizes the capture of the external field.

$$G_V = 1 + \frac{2 \frac{R_2}{L}}{1 + \frac{L}{R_1} S} \rightarrow S_1 = -\frac{R_1}{L} \quad (8)$$

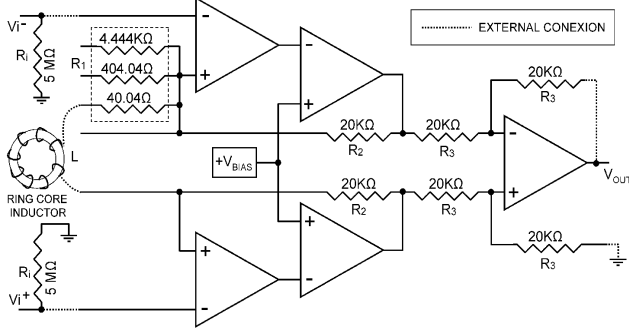


Fig. 7. Structure of the instrumentation amplifier, AD524.

The final amplifier stage was realized using the LM833 subsystem, which consists of two, low-noise operational amplifiers joined in cascade, sharing the gain between the two sub-stages such that the total gain of the system can be adjusted between 0 dB and 52 dB. Fig. 8 shows the final amplifier diagram that delivers the signal to the A/D converter.

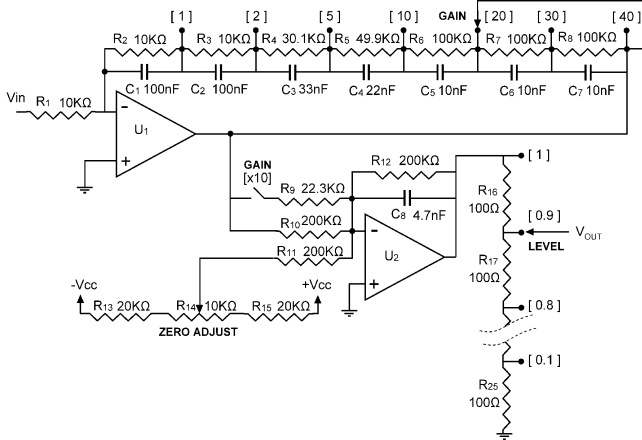


Fig. 8. Diagram of the final amplifier.

Amplifier  $U_1$  has an adjustable gain from 1 to 40, and its values are given in Table II. The capacitor array ( $C_1$  to  $C_8$ ) allows two poles to be maintained at 100 Hz for any of the gains selected.

TABLE II  
GAIN OF AMPLIFIER  $U_1$  IN THE FINAL STAGE

Gain	1	2	5	10	20	30	40
G(dB)	0	6	14	20	26	29.5	32

Amplifier  $U_2$  has a summing configuration to correct the zero adjustment before delivering the signal to the conversion stage. With the switch GAIN[x10], we can set the gain to 0 or 20 dB. Moreover, the resistance array ( $R_{16}$  to  $R_{25}$ ) of the output is configured as a volume selector that reduces the overall gain of the system. This adjustment is required so that no clipping occurs in the input stages of the A/D converter because the converter used has a narrower dynamic range than the dynamic

range of the amplifier. Table III shows the reduction factors of the output level.

The resistances  $R_{13}$  (10 K $\Omega$ ),  $R_{14}$  (20 K $\Omega$ ) and  $R_{15}$  (20 K $\Omega$ ) are used for the zero adjustment, given that the A/D converter introduces a certain direct component at its input.

TABLE III  
REDUCTION IN OUTPUT LEVEL

Reduction dB	1	0.9	0.8	0.7	0.6	0.5	0.4	0.3	0.2	0.1
	0	-0.9	-2	-3	-4.5	-6	-8	-10.5	-14	-20

#### D. Noise Study

With the test amplifiers, we proceeded to the theoretical calculation of the equivalent input noise RTI using the method provided by Art Kay in [32]. Then, we tested it with resistors of different input values, simulating the internal impedances of possible signal sources. The resistor values tested were 0 K $\Omega$  (short-circuit), 1.2 K $\Omega$ , 25 K $\Omega$ , 110 K $\Omega$ , 220 K $\Omega$  and 470 K $\Omega$ . The goal was to determine the *rms* noise and spectral distribution of the equivalent input noise (RTI) by comparing their behavior to different signal sources characterized by their internal impedance.

Table IV gives a summary of the data for calculating noise taken from the manufacturers' datasheets. The following noise components were used to calculate the equivalent noise Referred To the Input (RTI):

##### 1) From the sensor:

- The noise voltage corresponding to the equivalent resistance of the sensor ( $R_s$ ),  $en_{rb}$ .
- The influence of current noise on the instrumentation amplifier (IA),  $in$ . The latter can have two components: broadband  $in_{BB}$  and flicker  $in_f$ . This noise source is transformed to voltage when multiplied by the  $R_s$  of the sensor.

##### 2) From the instrumentation amplifiers:

- Broadband noise voltage,  $en_{BB}$ .
- Flicker noise voltage,  $en_f$ .

Once the sources have been identified and the operational bandwidth has been defined, the total equivalent noise at the input is expressed by equation (9); factor 2 is the result of the sensor being balanced differentially and the two branches that contribute noise.

$$RTI = \sqrt{2 \cdot en_{rb}^2 + 2 \cdot (in \cdot R_s)^2 + en_{BB}^2 + en_f^2} \quad (9)$$

In experimental calculations, the equivalent RTI is obtained by measuring the noise voltage at the output and by dividing it by the gain.

Table IV shows the noise source equivalent to the input RTI in real *rms* values for each resistance tested.

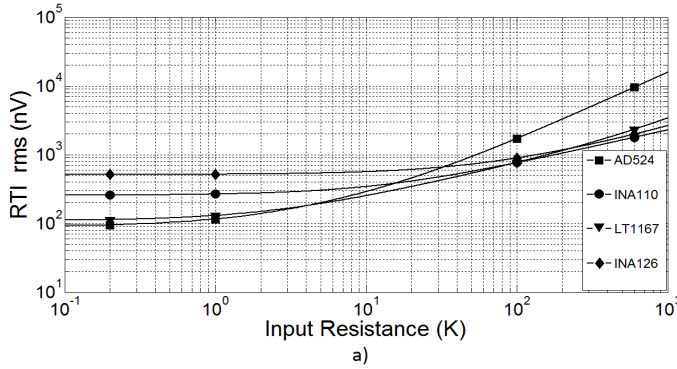
From Fig. 9, we can compare the results of the theoretical noise analysis (Fig. 9a based on the data in Table IV) with the data obtained in the tests (Fig. 9b based on the test data shown in Table V). There is clearly a close correlation between the calculated and measured values with the greatest fidelity provided by amplifier AD524.

TABLE IV  
FEATURES OF THE INSTRUMENTATION AMPLIFIERS

	AD524	INA110	LT1167	INA126
Noise voltage (nV/ $\sqrt{\text{Hz}}$ )	7	10	7.5	35
Flicker voltage (1Hz) (nV/ $\sqrt{\text{Hz}}$ )	10	100	25	200
Corner frequency (Hz)	2.5	600	7	30
Noise Current (fA/ $\sqrt{\text{Hz}}$ )	350	1.8	124	60
Flicker Current (1Hz) (fA/ $\sqrt{\text{Hz}}$ )	25000	-	400	200
Corner frequency (Hz)	30	-	40	30
Bandwidth (MHz)	25	40	12	1

Using the data obtained in the tests, we also calculated the input noise spectral density, displayed in Fig. 10. An analysis of these graphs allows the following conclusions to be drawn:

- Amplifier AD524 is the most suitable for signal sources



with a low internal impedance of approximately 1 K $\Omega$ .

- For high values of up to 100 K $\Omega$ , amplifiers INA110 and LT1167 give similar values.

- For values above 100 K $\Omega$ , the INA110 amplifier is ideal, providing an inappreciable current noise source compared to the other amplifiers and an absence of flicker noise.

TABLE V  
RMS NOISE MEASURED (nV) AT THE INPUT RTI

	Short	1.2 K $\Omega$	25 K $\Omega$	110 K $\Omega$	220 K $\Omega$	470 K $\Omega$
AD524	87.1	126.4	649.7	1996.4	3460.6	7302.2
INA110	177.3	201.9	474.1	933.2	1290.5	1830.9
INA126	406.3	416.3	573.9	940.7	1272.0	1806.0
LT1167	137.4	162.8	411.7	926.2	1453.1	2352.0

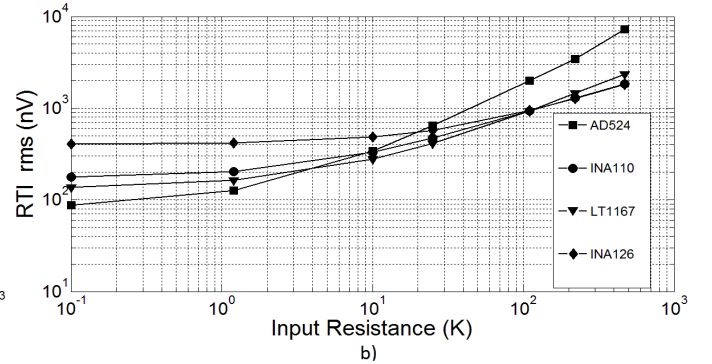


Fig. 9. Noise comparison of the four instrumentation amplifiers: a) theoretical, b) experimental.

#### IV. NOISE FLOOR ESTIMATE

To determine the S/N ratio in the experimental phase of real measurements using the sensor, it is necessary to determine the system noise floor as the sum of the thermal noise of the sensor, the total amplifier noise and the A/D converter noise. A more direct procedure is to isolate the sensor away from any external noise (in an anechoic chamber) and take measurements under the same conditions as the ambient radio signal (gain, averaging time, calibration, etc.). This method requires the availability of a chamber in the ELF range that must be large enough not to affect the sensor's features, which is a situation beyond our control. Another indirect method is to take measurements, substituting the sensor by resistances whose values match the real part of  $Z$  for the sensor at various frequencies within the range of measurement.

##### A. Analysis of the signal and noise in a coil

To determine the spectral distribution of the total noise at the output of the sensor, it is necessary to study the behavior of the coil. Analyzing the model of Fig. 1a, the output voltage of the coil is defined by the following equation:

$$V_{ab} = V_s \frac{1 - \omega^2 LC_L - j\omega C_L R_L}{(1 - \omega^2 LC_L)^2 + (\omega C_L R_L)^2} \quad (10)$$

On the other hand, the real part of the impedance presented by the coil meets the equation:

$$\text{Re}(Z_{ab}) = \frac{R_L}{(1 - \omega^2 LC_L)^2 + (\omega C_L R_L)^2} \quad (11)$$

Considering that  $Z_{ab}(\omega)$  of the sensor coil can be measured by the vector network analyzer and known data,  $V_{ab}$  can be expressed as a function of  $Z_{ab}$ :

$$V_{ab} = V_s \text{Re}(Z_{ab}) \frac{1 - \omega^2 LC_L - j\omega C_L R_L}{R_L} \quad (12)$$

In this particular case for setting the frequency of the sensor, the coil autoresonance is:  $\omega = \omega_0 = 1/\sqrt{LC_L}$

$$V_{ab}(\omega_0) = -jV_s \cdot \text{Re}(Z_{ab}) \sqrt{\frac{C_L}{L}} \quad (13)$$

Which shows that the induced voltage in a sensing coil is directly proportional with the real part of the sensor's impedance  $Z_{ab}$ . It also shows that the maximum of the voltage induced in the sensing coil occurs in the autoresonance frequency, which corresponds well with the maximum value of the real part of the impedance of the coil. In the case of sensor 3, the maximum is placed at 55 Hz, as shown in Fig. 2. Because noise is a signal that is induced in the coil, the spectral distribution of the voltage noise corresponds to that expressed in equation (12), and the maximum of the noise spectral distribution, which is present at the autoresonance frequency of the coil sensor, is stated in (13).

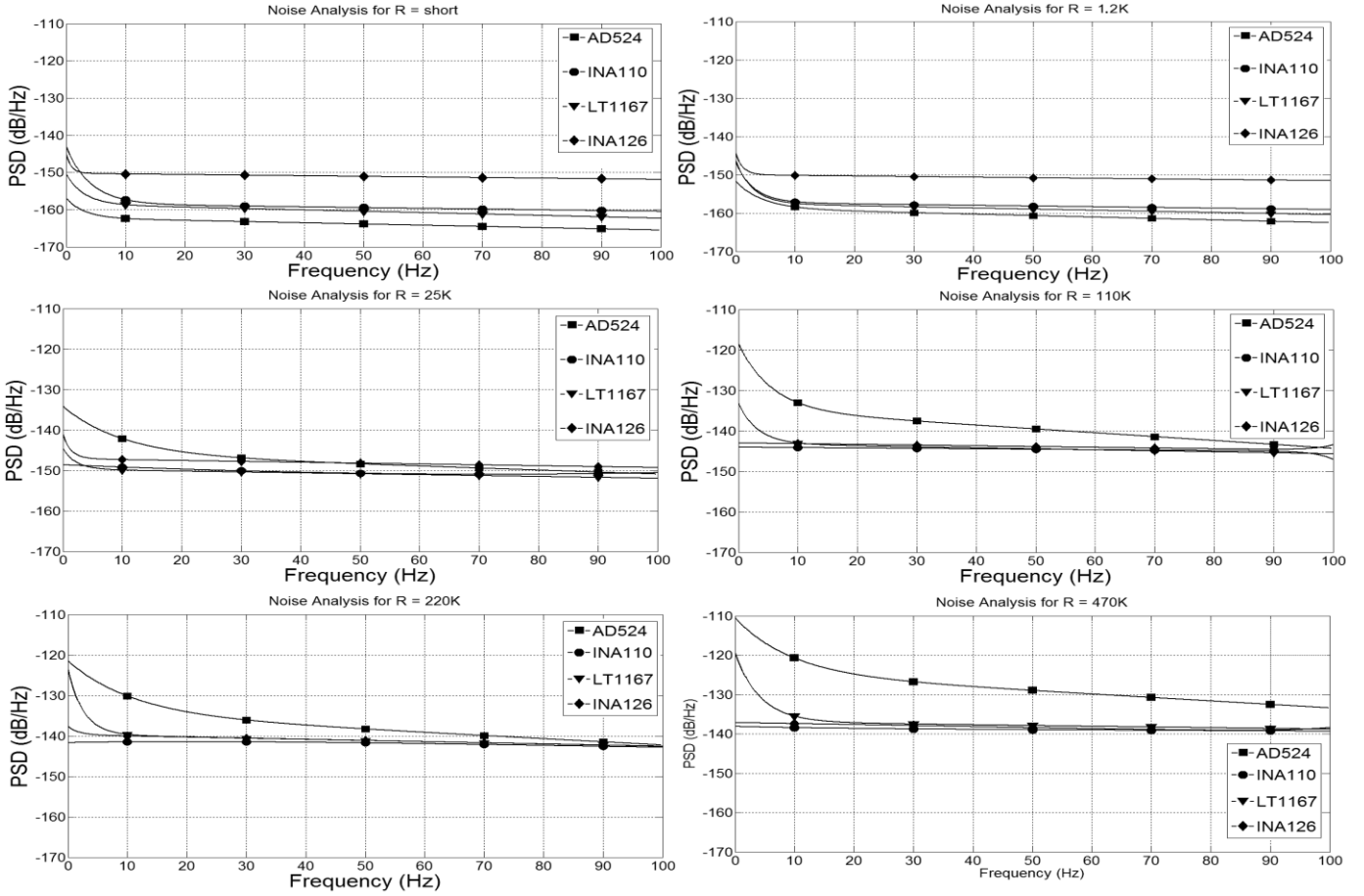


Fig. 10. Noise spectral density for different internal resistances at the source.

### B. Calculation of the Noise Floor

The indirect method is to take measurements, substituting the sensor by resistances whose values match the real part of  $Z$  for the sensor at various frequencies within the range of measurement. Using this method, we obtain the real value of the noise floor valid at frequencies corresponding to each resistor. For sensor 3, if one of the resistances selected corresponds to the maximum  $Re(Z)$ , (in this case at 55 Hz and also for upper frequencies), the dominant noise is the noise from the sensor because the impedance of the noise floor  $Z_{ab}$  is higher than  $1.5 \text{ M}\Omega$  (as shown in Fig. 2), and the noise voltage, in this case is indicated by equation (14), where  $k$  is a constant depending on the system of amplification.

$$V_n = k\sqrt{\text{Re}(Z_{ab})} \quad (14)$$

This adjustment is not valid close to the origin ( $f=0$ ), where the influence of the noise amplifier exceeds the noise from the sensor, given that  $Re(Z_{ab})$  is substantially lower. In this case, the previous curve is adjusted, forcing it to pass through various known correspondence points ( $Re[Z(f)]$  at 3 Hz,  $Re[Z(f)]$  at 10 Hz).

Table VI shows the level of the noise floor measured experimentally (only for sensor 3), connecting resistances to the input of the amplifiers. These resistances correspond to the ones seen by the amplifier at different frequencies, as if sensor 3 had been connected to the input.

The product of the measured noise signal, replacing the sensor by a resistor of equal value to the  $R_{ab}$ , and *Adjustment*

*Function* corrects the uncalibrated signal noise outside resonance and obtains the calibrated noise floor. Fig. 11 shows the calibration process of the noise floor. The adjustment function is used as an exponential function whose coefficients depend on the true value noise points (red in Fig. 11).

TABLE VI  
NOISE FLOOR CALIBRATION FOR THE FOUR AMPLIFIERS FOR DIFFERENT RESISTANCES

Frequency	$Re[Z(f)]$	AD524 (pT)	INA110 (pT)	LT1167 (pT)	INA126 (pT)
90 Hz	$1.5 \text{ M}\Omega$	$1.7 \cdot 10^{-1}$	$1.5 \cdot 10^{-2}$	$2.9 \cdot 10^{-2}$	$2.1 \cdot 10^{-2}$
55 Hz	$3.3 \text{ M}\Omega$	$1.5 \cdot 10^{-1}$	$1.5 \cdot 10^{-2}$	$2.8 \cdot 10^{-2}$	$2.0 \cdot 10^{-2}$
10 Hz	$220 \text{ K}\Omega$	$1.5 \cdot 10^{-1}$	$1.8 \cdot 10^{-2}$	$3.5 \cdot 10^{-2}$	$2.1 \cdot 10^{-2}$
3 Hz	$50 \text{ K}\Omega$	$2.0 \cdot 10^{-1}$	$3.0 \cdot 10^{-2}$	$3.8 \cdot 10^{-2}$	$3.4 \cdot 10^{-2}$

The adjustment function model proposed and used in this application is implemented by setting exponential functions. The  $A$ ,  $B$ , and  $C$  coefficients modify the amplitude, and the  $F_{C1}$ ,  $F_{C2}$ , and  $F_{C3}$  coefficients define the frequency to apply.

$$F_{adjust} = \left[ 1 + (A-1)e^{\frac{-f}{kF_{C1}}} \right] \cdot \left[ 1 + (B-1)e^{\frac{-f}{kF_{C2}}} \right] \cdot \left[ 1 + (C-1)e^{\frac{-f}{kF_{C3}}} \right] \quad (15)$$

Equation (15) shows the adjustment function model. The amplitude coefficients  $A$ ,  $B$ , and  $C$ , and the position coefficients  $F_{C1}$ ,  $F_{C2}$  and  $F_{C3}$  are calculated, so that the uncalibrated function matches in true value points. The constant  $k$  is chosen to correct

a slope of exponential change. In this case, we assign the value  $k = 7$ .

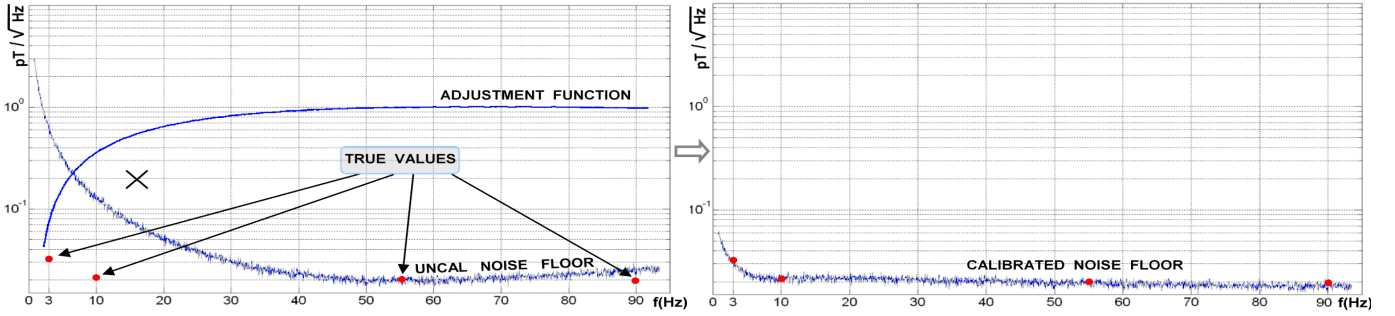


Fig. 11. Calibration process of the noise floor.

## V. RESULTS

Over the course of more than two years of operating the measurement system away from human activity, we have obtained a wealth of information. This information, properly processed, has been very useful in establishing objective criteria regarding the techniques for measuring Schumann resonances. Trials were performed using four different instruments on the first stage amplification but ultimately used the same amplifier to be able to make a comparative study. The measurements were taken using sensor 3, comprising 300000 turns of wire that was 0.15 mm in diameter and grouped into four windings with a 2-meter-long core. The total gain was maintained at 66 dB and was adjusted to optimize the quality of the capture, achieving maximum amplification with minimal clipping. Fig. 12 shows the signal aspects in the time domain, sampled with a 24-bit A/D converter and a dynamic range of  $\pm 2.5$  Volts. Fig. 12a shows a correct adjustment of the gain, fixed at 66 dB ( $G_{A.I.} + G_{A.END}$ ), while Fig. 12b indicates excessive gain, which results in false spectra in the frequency domain, due to the clipping effect.

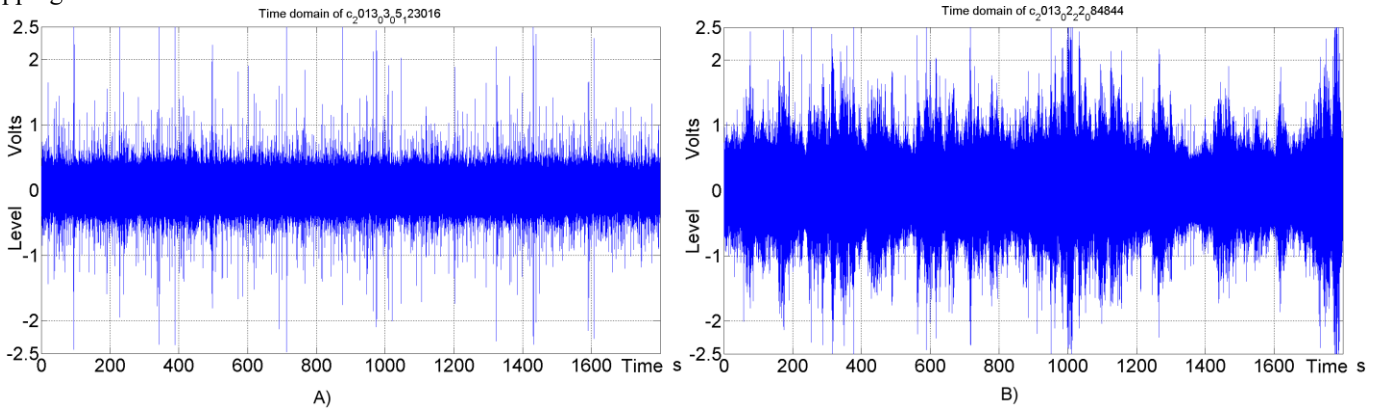


Fig. 12. Time domain signal: a) capture with adequate gain, b) capture with excessive gain.

In the graphs in Fig. 13, we can see the first three modes with their greater amplitude, coincide with the references consulted. The remaining resonances are generally much more subdued, and the bandwidth is 100 Hz.

As a means of comparison, we can use the difference between the level of the mode of the first resonance and the level of the system noise floor at the same frequency ( $\approx 7.5$  Hz). In this case, we obtain the following data: with the AD524, 20

The selection of four measurements was made over 30 minutes, each using a different instrumentation amplifier in the frequency domain, as shown in Fig. 13. Each graph shows both the ambient radio signal and the system noise floor of the measurement. To obtain the record of the system noise floor, the sensor was substituted by the main electric supply, whose real part of the impedance coincides with that of the sensor in the frequency range 0 to 100 Hz, when it is isolated to avoid the capture of external fields. All of the captures were subject to the same spectral averaging procedure using temporal windows, which is the norm when studying Schumann resonances. The measurements were chosen to have a similar level of ambient signal for each amplifier to achieve objective comparisons. As seen in Fig. 13, the noise level of the system (including the noise of the sensor itself) is well below the signal level detected by the sensor for every case, even with the low-cost amplifier INA126. This indicates that any commercial instrumentation amplifier is suitable for this purpose.

dB and with the INA110, 39 dB; using the LT1167 and INA126, 31 dB. A very important factor for these results is the sensitivity of the sensor. In cases using smaller sensors with less sensitivity, the system noise floor cannot be overcome at some frequencies. The lowest frequencies are the most susceptible to this because of flicker noise. The amplifiers with lower current noise perform better in this application.

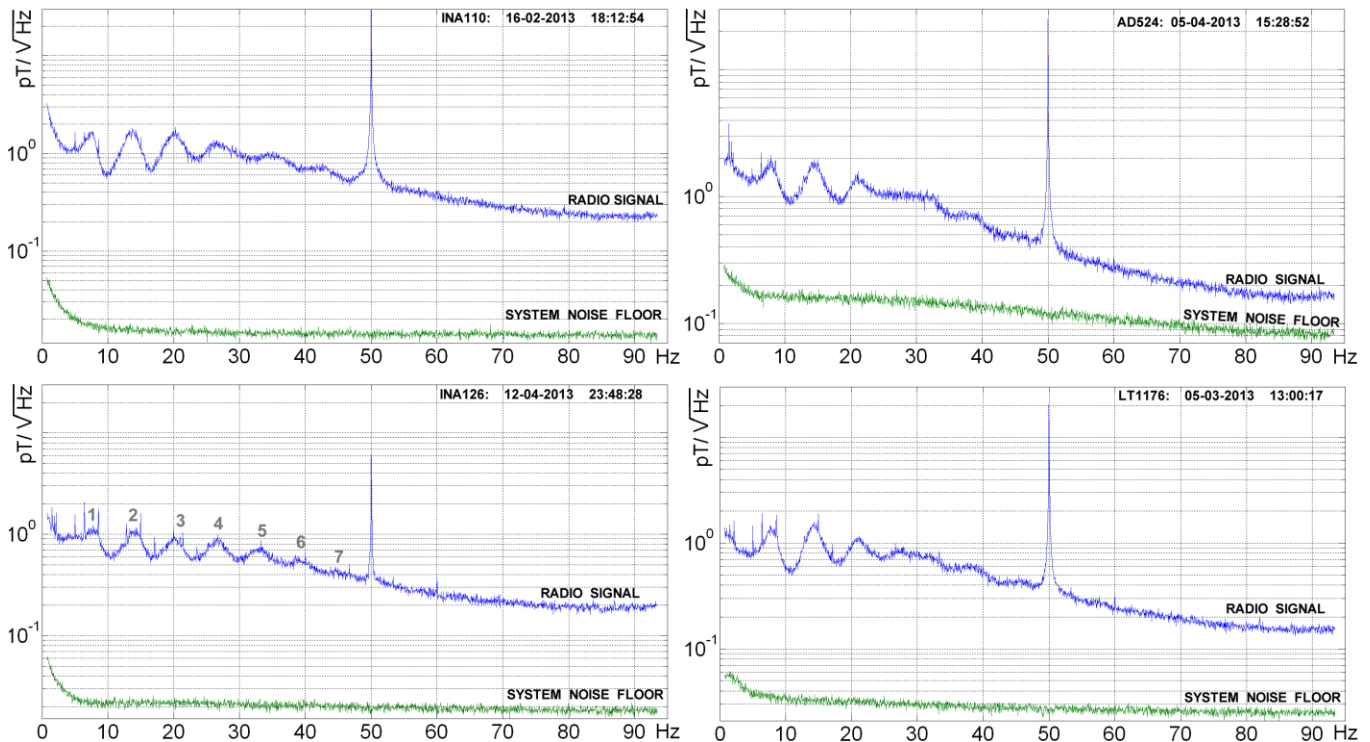


Fig. 13. Spectral averaging and system noise floor in the four amplifiers for 30 minute captures.

## VI. CONCLUSIONS

Published studies that are state of the art for measuring Schumann resonances reflect the interests of the researchers but do not consider improvements to the systems of measurement. Optimization of this system allows better records and shorter averaging times. We propose an optimized system of amplification for bettering the signal to noise ratio, and consequently the averaging time. The first stage of this system is an instrumentation amplifier with a balanced input for the sensor and cable. We conducted a comparative study of four devices that are available from three brand leaders. Analyzing the results of more than one year of measurements, we can draw the following conclusions:

1. The type of instrumentation amplifier is not a critical factor for the correct measurement of Schumann resonances so long as the sensor supplies a sufficient level of ambient radio signal, and the instrumentation amplifier (IA) linearity is sufficient to avoid artifacts in the true spectra at higher frequencies. The offset does not affect this application, and the CMRR is not of great significance. Low-cost (3\$) devices are sufficient.

2. An IA that optimizes noise in the current regime is more suitable for sensors with a large number of windings of thin wire and exhibits high values for the real part of the impedance. Meanwhile, the instrumentation amplifiers that optimize noise in the voltage regime are better when the sensors have fewer turns, and the wire is thicker.

3. The averaging time must be as short as possible because we detected significant variations in the results of captures separated by 30 minutes.

4. It is very important to precisely tune the level of amplification for all stages. Determining the optimal setting

may require several days of records. Using compression systems (such as A Law) to place more weight on the weak signals without clipping the strong signals does not yield good results because deviation from linearity means that restoration without an artifact is impossible.

5. The digitization stage must have the highest resolution as possible: 24 bits is sufficient to allow weak signals to be recorded with adequate converter-account because the Schumann Resonances have relatively low amplitude compared to the natural ambient radio noise level. Furthermore, there must be a sufficient dynamic range to avoid clipping –in accordance with the previous conclusion. The signal of interest occupies approximately 1/5 of the dynamic range.

6. The method of estimation of the noise floor, without the free signals sensor connected, yielded experimental results that provide validation and allows measurements of the Schumann resonances with assured quality with captures of only 30 minutes, as shown in Fig. 13.

It should be noted that the results obtained with the instrumentation amplifiers are pertinent to this particular application. For other applications with a broader bandwidth or lower input impedance (audio, PT100, etc.), the results would be different.

The solutions adopted are highly satisfactory: in the Calar Alto ELF observatory, we were able to measure the first seven resonance modes (the eighth coincides with the 50 Hz electrical power lines) with acquisition times of 15 to 30 minutes and with a signal-to-noise ratio in the fundamental mode of 39 dB, as evident in Fig. 13.

## ACKNOWLEDGMENTS

This work was forms part of Project TEC-2009-13763-C02\_02 and FQM-32080 funded by the Ministry of Economic y Competitiveness of Spain and Innovation, Science and Enterprise (Andalusian Regional Government). It was also funded from the European Union FEDER program, as part of Research Group TIC-019 "Electronics, Communications and Telemedicine", University of Almeria. Also our thanks to the Andalusian Institute of Geophysics for the joint use of facilities at Calar Alto.

## REFERENCES

- [1] W. O. Schumann, "Über die Strahlunglosen Eigenschwingungen einer leitenden Kugel die von Luftschicht und einer ionosphärenhle umgeben ist," *Z. Naturfoschaftung*, vol. 7, 1955, 149-154.
- [2] Z. Niecekarz, A. Kulak and S. Zieba, "Comparison of global storm activity rate calculated from Schumann resonance background components to electric field intensity Eoz," *Atmospheric Research*, vol. 91, no. 3, Mar. 2009, pp. 184-187.
- [3] A. P. Nickolaenko, "ELF radio wave propagation in a locally no uniform earth-ionosphere cavity," *Radio Science*, vol. 29, no. 5, 1994, pp. 1187-1199.
- [4] E. R. William, "Schumann Resonance a global tropical thermometer," *Radio Science*, vol. 256, no. 5060, May. 1992, pp. 1184.
- [5] T. Bleier and F. Freund, "Earthquake Alarm," *IEEE Spectrum*, vol. 3, Dec. 2005, pp. 21-25.
- [6] A. P. Nickolaenko, M. Hayakawa and Y. Hobara, "Schumann Resonances and global lightning activity," *Mathematical Methods in Electromagnetic Theory*, vol. 1, June. 1998, pp. 296-297.
- [7] K. Sao, M. Yamashita and S. Tanashashi, "Experimental investigations on Schumann resonance frequencies," *Electronics and communications in Japan*, vol. 56, no.6, June. 1973, pp. 80-85.
- [8] F. Simões and M Rycroft, "Schumann resonances as a means of investigating the electromagnetic environment in the solar system," *Electronics and communications in Japan*, vol. 137, no. 1-4, June. 2008, pp. 455-471.
- [9] A. P. Nickolaenko, "Application of the Hurst exponent in the analysis of natural ELF electromagnetic noise," *Proceedings of MMET'00, VIII-th International Conference on Mathematical Methods in Electromagnetic Theory*, vol. 1, 2000, pp. 638-640.
- [10] E. I. Yatsевич, A. V. Shvets and L. M. Rabinowich, "Results of comparing Schumann-Resonance observations with the model of a Single Global thunderstorm center," *Radiophysics and Quantum Electronics*, vol. 48, no. 4, April. 2005, pp. 254-267.
- [11] Y. Tulunay, E. Altuntas and E. Tulunay, "A Case Study on the ELF Characterization of the Earth-Ionosphere Cavity: Forecasting the Schumann Resonance Intensities," *The Neural Network Technique*, vol. 33, Oct. 2007, pp. 983-987.
- [12] V. G. Bezrodny, "Magnetic polarization of the Schumann resonances: An asymptotic theory," *Journal of Atmospheric and solar-terrestrial Physics*, vol. 69, March. 2007, pp. 995-1008.
- [13] A. P. Nickolaenko, "Universal Time and Local Time Variations," *Geophysical Research*, vol. 27, no.19, 2005, pp. 3185-3188.
- [14] J. Rai, R. Chand, M. Israil, S. Kamakshi, "Studies on the Schumann resonance frequency variations," *Proc. of EUCAP 2009 European Conf. on Antennas and Propagation*, vol. 256, no. 5060, 2009, pp. 1437-1440.
- [15] C. Bing-Xia and Q. Xiao-Lin, "Observations on Schumann Resonance in Low Ionosphere," *Journal of Electronics and Information Technology*, vol. 8, no. 6, Aug. 2003, pp. 627-630.
- [16] M. Füllekrug, "Detection of thirteen resonances of radio waves from particularly intense lightning discharges," *Geophysical Research Letters*, vol. 32, no. 13, L13809, doi:10.1029/2005GL023028, 2005.
- [17] A. Kruger, "Construction and Deployment of an ULF Receiver for the Study of Schumann Resonance in Iowa," [Online]. Available: <http://ihr.uiowa.edu/projects/schumann/Index.html>.
- [18] F.P. Sierra, H.S. Vazquez, et al "Development of a Schumann-Resonance Station in Mexico: Preliminary Measurements," *IEEE Antennas and Propagation Mag.*, vol. 40, no.3, pp 112-119, Jun. 2014.

- [19] J.K. Hwang and P.N. Markham, "Power System Frequency Estimation by Reduction of Noise Using Three Digital Filters," *IEEE Trans. Ins. Meas.*, vol. 63, no 2, pp. 402-409, Feb. 2014.
- [20] Felix A. Levinzon, "Ultra-Low-Noise High-Input Impedance Amplifier for Low-Frequency Measurement Applications" *IEEE Trans. Circuits Syst. I, Regular Papers.*, vol. 55, no. 7, pp. 1815-1822, August. 2008.
- [21] A.Roshan-Zamir and S.J. Ashtiani, "A New Method for Measurement of Low-Frequency Noise of MOSFET," *IEEE Trans. Ins. Meas.*, vol. 62, no 11, pp. 2993-2997, Nov. 2013.
- [22] E. Serrano and R. Pallas, "Noise Reduction in AC-Coupled Amplifiers," *IEEE Trans. Ins. Meas.*, vol. 63, no 7, pp. 1834-1841, Jul. 2014.
- [23] R. M. García, J. A. Gazquez and N. Novas, "Characterization of high-value inductors in ELF Band using a Vector Network Analyzer," *IEEE Trans. Ins. Meas.*, vol. 62, no. 2, Feb. 2013, pp. 415-423.
- [24] J. G. Proakis and D. G. Manolakis. "Tratamiento digital de señales," Prentice Hall, 3<sup>a</sup> edition, 1998.
- [25] Impedance Measurement Function E5061B-005. Agilent Technologies. Dec. 2010.
- [26] B. Whitlock, "Balanced Lines in Audio Systems: Fact, Fiction, and Transformers," *JAES*, vol. 43, no. 6, June. 1995, pp. 454-464.
- [27] A. Soliman, "New Active RC configuration for realising a medium-selectivity Notch Filter," *IEE Electronis Letter*, vol 8 no 21, Oct. 1972, pp 522-524.
- [28] Analog Devices AD524 datasheet. Available: [http://www.analog.com/static/imported-files/data\\_sheets/AD524.pdf](http://www.analog.com/static/imported-files/data_sheets/AD524.pdf)
- [29] Texas Instruments INA 110 datasheet. Available: <http://www.ti.com/lit/ds/symlink/ina110.pdf>
- [30] Texas Instruments INA 126 datasheet. Available: <http://www.ti.com/lit/ds/symlink/ina126.pdf>
- [31] Linear Technologies LT1167 datasheet. Available: <http://cds.linear.com/docs/en/datasheet/1167fc.pdf>
- [32] A. Kay, "Operational amplifier noise: Techniques and tips for analyzing and reducing noise," Elsevier, 1<sup>st</sup>edit. ISBN: 978-0-7506-8525-2. 2012.

## Biographies



**José A. Gázquez Parra** (M'02) (SM'12) received his Ph.D. degrees in Telecommunication Engineering from the University of Malaga. He has been associate Professor in the Electronic and Computers Technology Department at the University of Granada (Spain) (1990-1993) and currently is professor in the Engineering Department at the University of Almeria (Spain) since 1994. He was on the board of the company Engineering and Remote Control S.A. (Granada) (1991-1994). He is principal researcher of the Electronic Communications and Telemedicine (TIC019) Research Group of the Andalusian Research Plan. His research interest includes electronic design, measurement systems, telecontrol and embedded systems in real time. (email: [jgazquez@ual.es](mailto:jgazquez@ual.es)).



**Manuel Fernandez Ros** received his degree in Telecommunication Engineering from the University of Alcalá de Henares (Madrid). He teaches Electronics System in the Consejería de Educacion, Andalusia Region. His research includes DSP (digital signal processing) systems and electromagnetic phenomena. (e-mail: [mfr460@ual.es](mailto:mfr460@ual.es)).



**Nuria Novas Castellano** received her Ph.D. degrees in Electronic Engineering from the University of Almeria. She is currently an Associate Professor in the Engineering Department at the University of Almeria (Spain) since 1999 and her research includes control systems and measurement. (e-mail: [nnovas@ual.es](mailto:nnovas@ual.es)).



**Rosa M García Salvador** received her Ph.D degree in Physics from the University of Almeria. Since 2012, she has been a research and teaching assistant in the Engineering Department at the University of Almeria and her research includes measurement systems and electromagnetic phenomena (email: [rgs768@ual.es](mailto:rgs768@ual.es)).